Ionic Coulomb blockade controls the current in a short narrow carbon nanotube

William A. T. Gibby,[1] Miraslau L. Barabash,[2] Igor A. Khovanov,[3] Dmitry G. Luchinsky,[1] and Peter V. E. McClintock*[1]

[1)] *Department of Physics, Lancaster University, Lancaster LA1 4YB, UK*
[2)] *Department of Chemical Engineering, University College London, WC1E 6BT, UK*
[3)] *School of Engineering, University of Warwick, Coventry, CV4 7AL, UK*

(*Electronic mail: p.v.e.mcclintock@lancaster.ac.uk)

(Dated: 7 August 2024)

We use all-atom molecular dynamics simulations to investigate ionic conduction in a short, charged, single-wall carbon nanotube. They reveal ionic Coulomb blockade (ICB) oscillations in the current as a function of the fixed charge on the wall, and an associated occupancy staircase. Current peaks related to fluctuations around the 2→1 and 1→0 steps in occupancy are clearly resolved, in agreement with ICB theory. Current peaks were also observed at constant occupancy. These unpredicted secondary peaks are attributed to edge effects involving a remote knock-on mechanism; they are attenuated, or absent, for certain choices of model parameters. The key parameters of the system that underly the current oscillations are estimated using ICB theory and the potential of the mean force. Future perspectives opened up by these observations are discussed.

I. INTRODUCTION

Biological ion channels are vital to living creatures and are widely targeted in pharmacology through the development of channel-specific drugs[1–3]. Artificial ion channels, their close analogues, are expected to shape the next generation of nanodevices for DNA sequencing[4], nanoscale energy harvesting[5,6], desalination[7], gas[8] and isotope[9] separation, and molecular sensors. However, understanding, predicting and controlling charge transport in ion channels still present formidable challenges to both nanotechnology[10] and biophysics[1,11]. Critical gaps recently identified[12,13] in our understanding of ionic conduction in nano-channels include correlated transport and the conditions needed for the enhanced selectivity of particular ions. Coulomb blockade[14–18] is perhaps the best-known phenomenon believed to underlie the selectivity and conductivity properties of nano-channels.

Ionic Coulomb blockade (ICB) is the ion-related counterpart of electronic Coulomb blockade, which controls transport in single-electron transistors and other quantum devices[19–22] and is widely observed in man-made nanostructures[23]. Both the electronic and ionic CBs are essentially classical electrostatic phenomena[16,24] related to the fact that, on the nanoscale, the capacitance of the system $C_{\rm dot}$ becomes very small. Consequently, both the total electrostatic energy $\mathscr{E}$ and the Coulomb charging energy $U_{\rm c}$[16,19–21] may significantly exceed the thermal energy:

$$\begin{aligned} \mathscr{E} &= \frac{(nzq+Q_{\rm ex})^2}{2C_{\rm dot}} = U_{\rm c}(n_{\rm ex}\pm nz)^2, \quad \text{where} \\ U_{\rm c} &= \frac{q^2}{2C_{\rm dot}} \gg k_{\rm B}T. \end{aligned} \tag{1}$$

Here $z=1$ and $q=-e$ for electronic Coulomb blockade while $z=1,2,...$ and $q=\pm e$ for ICB[15–18], where e is the elementary charge, and n is the number of mobile charges; $Q_{\rm ex}=n_{\rm ex}e$ is an externally controlled charge, either on the channel wall in the ionic case, or induced by the gate voltage on the quantum dot in the electronic case. As a result, the conducting device can accommodate only a small, discrete, number of charged particles.

The electrostatic potential of the system is shown in Fig. 1 (a) as global minima of the discrete set of parabolic potentials given by Eq. (1) for different values of *n vs.* $Q_{\rm ex}$. Minima of the global potential correspond to stable states with corresponding minima in the permeating current and a fixed number of mobile charges in the channel, resulting in occupancy plateaus as shown in (b). At the peaks of the potential there are fluctuations between n and $(n+1)$ in the number of mobile charges, yielding peaks in channel current at the edges of occupancy steps. The lines correspond to strong (dashed) and weak (solid) ICB effects[16]. Full blockade (i.e. zero conduction at minima) is attained when $U_{\rm c} \gg 1\ k_{\rm B}T$, but the effects are much weaker when $U_{\rm c} \sim \mathscr{O}(1\ k_{\rm B}T)$. This approach immediately demonstrates the deep analogy that exists between ICB and electron transport in single electron devices[20,21,25,26] and it predicts Coulomb blockade and oscillations in ionic transport through narrow channels.

The analytic predictions in Fig. 1 (b) show that the current is blocked for small $Q_{\rm ex}$, while current oscillations and the corresponding occupancy steps as a function of wall charge occur for larger negative values of $Q_{\rm ex}$. Similar behaviour was predicted analytically[18] in long channels conducting hydrated ions. As mentioned above, changing $U_{\rm c}$ affects the shapes and locations of the peaks/steps. This effect was noted in[15], and is described as weak/strong Coulomb blockade: see also[27] and the supplementary material (SM).

Ionic Coulomb blockade without oscillations was initially predicted in 2D nanopores using a kinetic model[14]. ICB and current oscillations were later predicted in a wide range of biological selectivity filters (including KcsA and NaChBac[27]) and in carbon nanotubes[18,27].

Feng *et al.*[17] observed an experimental indication of ICB in 2D nanopores, but the strongly nonlinear current-voltage characteristics that they observed should probably not be considered as an unequivocal demonstration of ICB[28]. A systematic

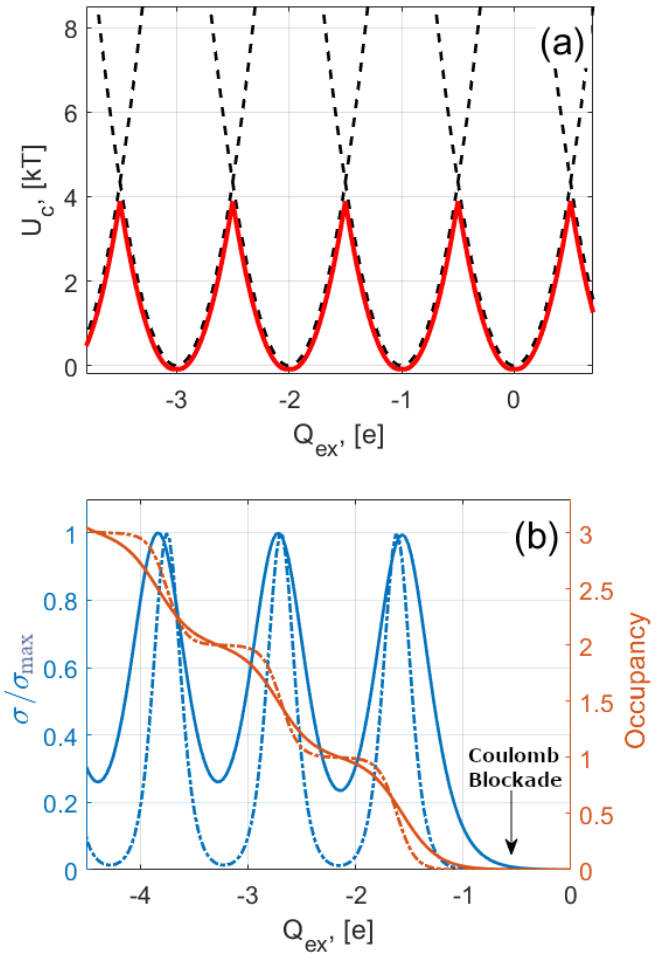

FIG. 1. (a) Electrostatic potential of the system U_c as a function of the wall charge Q_{ex}. Dashed lines represent the parabolic potential given by Eq. (1) for each n, and the full red line plots the global minimum of the potential. (b) Conductivity oscillations (blue) and population steps (orange) predicted by the statistical theory[27] for $U_c = 10.2\ k_B T$ (dashed-dotted lines) and $U_c = 3\ k_B T$ (solid lines).

sequence of mutation experiments, and an elaborated analysis[29] showed that ICB oscillations apparently underlie the observed mutation-induced transformations of selectivity and conductivity in biological sodium and calcium filters. However, full ICB oscillations could not be observed, either in the experiments or in the corresponding molecular dynamics (MD) simulations. The latter constitute an important link between theory and experiment. Specifically, the experimental observation of ICB[17] was confirmed by MD analysis[30] demonstrating the trapping and blocking of conducting ions in graphene-embedded 18-crown-6 ether pores followed by sharp increases of conduction via a knock-on mechanism at large bias voltage. In[17,31] blockade was measured as a function of voltage, preventing observation of ICB oscillations.

A single strong current peak as a function of rim charge Q_{ex}, and corresponding transitions of the ion translocation mechanism from the diffusion regime to knock-on in these structures, was observed in[32] at $Q_{ex} = -3.24e$. Similarly, a peak in the potassium conductivity through a charged graphene nanopore was observed in[33]. Closely related changes in the selectivity and conductivity mechanisms, depending on the charge and the arrangement of a functionalized graphene nanopore[34] also suggest that ICB can be observed in nanopores. However, observation of ICB current oscillations has remained elusive[17,28].

Here, we seek evidence of ICB oscillations in a charged carbon nanotube (CNT). These structures[18,27,35–38] are in themselves of special interest because they are widely used in nanofluidics e.g. to sequence single-stranded DNA[36], and to build field-effect transistors[39], ion[40] and water[41] pumps. They can be integrated with biological nanopores[42]. Their structural and functional similarity to biological selectivity filters suggests that CNTs may serve as useful biomimetic devices to reproduce biological functionality in nanotechnology systems[35–37].

We approach the problem by implementing all-atom molecular dynamics simulations of ionic conduction in a short, single-wall, carbon nanotube with charged walls.

II. MODELLING AND ALL-ATOM SIMULATION

To study ion conduction through the CNT we have developed an atomistic model of the system shown in Fig. 2, including graphene sheets, and a CNT connecting two bulk solutions with TIP3[43] water molecules and Joung-Cheatham[44] ions. The model was built using J-OCTA software[45] and a mixed force field: (i) Amber20[46] for water, ions, and graphene sheets; and (ii) the DREIDING force field[47] for the CNT. The simulations were performed with GROMACS software[48] using the NPT ensemble with a 2 fs time step.

The potential of the mean force (see above and the Supporting Information) was calculated using the well-tempered metadynamics approach[49] implemented in the GROMACS Colvars module[50]. One or two ions for estimating the 1-D or 2-D potentials were kept in a cylinder of 10 Å radius and placed on the tube's axis of symmetry. Other ions were excluded from the cylinder entrance by a repulsive potential.

Theoretical analysis considered ionic conduction through a set of binding sites connected sequentially[27]. The conductivity of the system was calculated by analysing the fluctuation intensity in the number of ions at each site, taking into account correlations of ionic fluctuations at different sites. The susceptibility was calculated using linear response theory, by expanding the mean occupancy of a binding site to the first order approximation with respect to the applied potential. The predictions of Fig. 1 were made for 5 identical binding sites able to accommodate up to 4 ions. The theory was also applied to estimation of the model parameters.

The graphene sheets separating the CNT from the bulk solutions have nanopores that allow for non-selective passage of ions from the bulk to the CNT. These nanopores are almost round in shape, with vertical and horizontal openings of 13.3 and 12.85 Å respectively. Their charged rims play the role of the charge found at the pore entrances of biological channels,

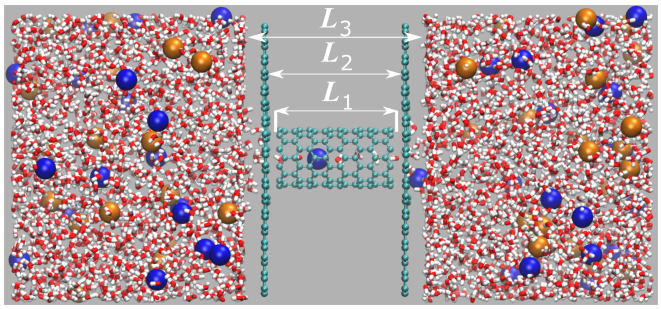

FIG. 2. The model. Potassium ions are shaded blue and chloride ions are shaded orange. The CNT and graphene sheets are shown with cyan atoms and bonds[51]. Water molecules are shown as red/white capsules. The arrows indicate respectively the lengths of the CNT (L_1 = 15.4 Å), of the channel between the graphene sheets (L_2 = 19.5 Å), and of the extended channel including the (effective) mouths on both sides (L_3 = 23.5 Å).

thus mimicking the internal and external vestibules of biological channels. Their geometry in the present study remains fixed. The total charge of the rim atoms is $Q_{\rm np} = -1.92e$. A constant electric field of either 0.04 or 0.08 V/nm is applied in the z-direction. The charged carbon atoms of the CNT (reddened in Fig. 2) are in the form of rings, mimicking the binding sites of the biological KcsA potassium channel. Note that, although the charge distribution might affect the magnitude of the permeating current, it would not be expected to affect the ICB phenomena that are of interest here.

The model is *conceptual*. It was developed to seek evidence for ICB oscillations. Because they were predicted[15,16,18,27,29,52,53] to occur over a wide range of parameters, we allowed for variations in the charge and Lennard-Jones parameters of the atoms. The distribution of the compensating charge and further details of the model are provided in the SM. We now discuss the results obtained.

III. RESULTS AND DISCUSSION

Simulations of the current through the CNT as a function of wall charge $Q_{\rm ex}$ for two different applied fields yielded the results shown in Fig. 3. Several features predicted by the theory are immediately evident. A region of complete Coulomb blockade occurs at small negative values of $Q_{\rm ex}$. The occupancy of the CNT (shown by blue circles) is integer, and changes from zero to one, and from one to two, in steps as $Q_{\rm ex}$ becomes more negative. Current peaks corresponding to these occupancy steps are clearly resolved, as indicated by black arrows in the figure. According to theory[15,16,18,27,29,52,53], the first peak is related to single-ion transitions as shown in video No. 1 of the SM, while the second peak corresponds to the 2→1 knock-on mechanism shown in video No. 3 of the SM. All of these features have long been anticipated on the basis of ICB theory[15,16,18,27,52], but had not hitherto been demonstrated.

However, a number of unexpected features are also evident in the MD simulations. First, the observed separation

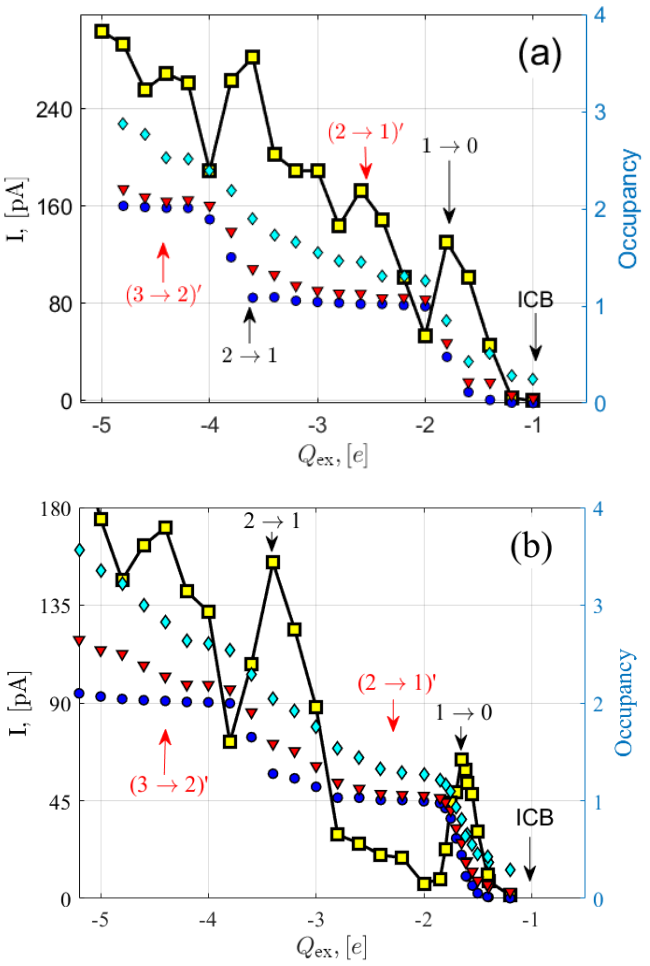

FIG. 3. Current through the CNT (yellow squares) and its occupancy (dark blue circles) as functions of the surface charge $Q_{\rm ex}$ for applied fields of (a) $F = 0.08$ V/nm and (b) $F = 0.04$ V/nm. The red triangles correspond to the occupancy of the region between the graphene sheets. The cyan diamonds show the occupancy of the system extended by 2 Å on both sides of the graphene sheets. The black and red vertical arrows indicate the locations of the main and secondary current peaks, respectively.

of the occupancy steps in terms of the wall charge is significantly larger than the value $Q_{\rm ex} \approx 1e$ expected from ICB theory for monovalent ions[15,16,18,27,29]. Secondly, additional current peaks (secondary peaks) may appear for constant values of occupancy as indicated by red arrows in the figure. Comparison of the current for the two different applied fields in (a) and (b) shows that the secondary peaks are not always present. For example, the $(2 \to 1)'$ peak is suppressed for $F = 0.04$ V/nm. We now consider in more detail the ionic dynamics responsible for each set of peaks, considering them in turn from right to left, and we will show that they correspond to two different types of conduction.

The potentials of the mean force (PMF) for a single ion transition $(1 \to 0)$ are shown in Fig. 4 (a) for three different values of the wall charge $Q_{\rm ex}$. Details of the calculations are provided in the SM Sec. 3. A key feature of the equilibrium

PMF shown in Fig. 4 (a) is the existence of high dehydration barriers at the channel entrance and exit. An increase in Q_{ex} reduces the entrance barrier but, at the same time, deepens the potential well within the channel, thus making it difficult for the ion to traverse the CNT. An external field (Fig. 4 (b)) biases the potential, helping ions to slide through the CNT. It also reduces both dehydration barriers, making the ionic transition nearly barrierless for the optimal values of $Q_{ex} = -1.6e$ and $F = 0.04$ V/nm. Sub-optimal values of the wall charge increase either entrance ($Q_{ex} = -1.4e$) or exit ($Q_{ex} = -1.8e$) barrier thus reducing the current. The optimal applied field corresponds to an equal probability of the CNT being occupied by either one or zero ions, thereby maximising the current peak. These features are in agreement with the predictions of ICB theory[15,16,18,27,29]. An illustration of this type of transition is given in video No. 1 of the SM.

For comparison, the 1D PMF for the transition peak $(2 \to 1)'$ is shown in Fig. 4 (b) for three values of applied field. First, we notice significant deepening of the potential well in the CNT, of up to $-20\ k_BT$ so that, even in the presence of the $F = 0.04$ V/nm applied field, the height of the barrier at the CNT exit is $\sim 10\ k_BT$. As a consequence the ion cannot leave the CNT without the assistance of a second ion. At the same time the occupancies of the CNT and of the channel between two graphene sheets practically do not change (see blue circles and red triangles in Fig. 3), indicating that the 2nd ion enters the CNT only very briefly to knock out the 1st ion. Additional studies discussed in the SM Sec. 4 confirm that such behaviour represents a remote knock-on conduction mechanism[54,55] when the 2nd ion knocks the 1st ion out of the CNT while still remaining at the channel mouth. This process becomes possible due to the enhanced ion-ion interaction within the CNT[56]. We note that such a mechanism is likely to be responsible for pushing ions from the S1-S3-S5 to the S0-S2-S4 configuration of the KcsA filter[57] where S0 and S5 are the external and internal vestibules of the KcsA filter, which correspond to the channel mouths of our model: see the SM Sec. 4 for further discussion.

Note in Fig. 3 (b) that the exit barrier, of $\sim 10\ k_BT$ for $F = 0.04$ V/nm, is too high even in the presence of the remote knock-on mechanism, so that the $(2 \to 1)'$ conduction peak is correspondingly suppressed. When the applied field is increased to $F = 0.08$V /nm, however, the exit barrier decreases to $3\ k_BT$ and the $(2 \to 1)'$ peak is then clearly resolved. Thus the remote knock-on mechanism is able to explain both the origin of this secondary current peak and the fact that it does not always appear.

A very similar physical picture underlies the dynamics of the $(2 \to 1)$ and $(3 \to 2)'$ transition peaks located at $Q_{ex} = -3.6e$ and $= -4.4e$, respectively. The $(2 \to 1)$ peak belongs to the set of classical ICB oscillations predicted by the theory, like the $(1 \to 0)$ peak discussed above. It is located at the population step from 1 to 2 corresponding to the intersection of the second and third branches of the electrostatic energy (1) shown in Fig. 1 (a). And, as expected during this transition, the CNT contains either one or two ions with equal probability: see video No. 3 of the SM.

Finally, the peak $(3 \to 2)'$ located at $Q_{ex} = -4.4e$ occurs

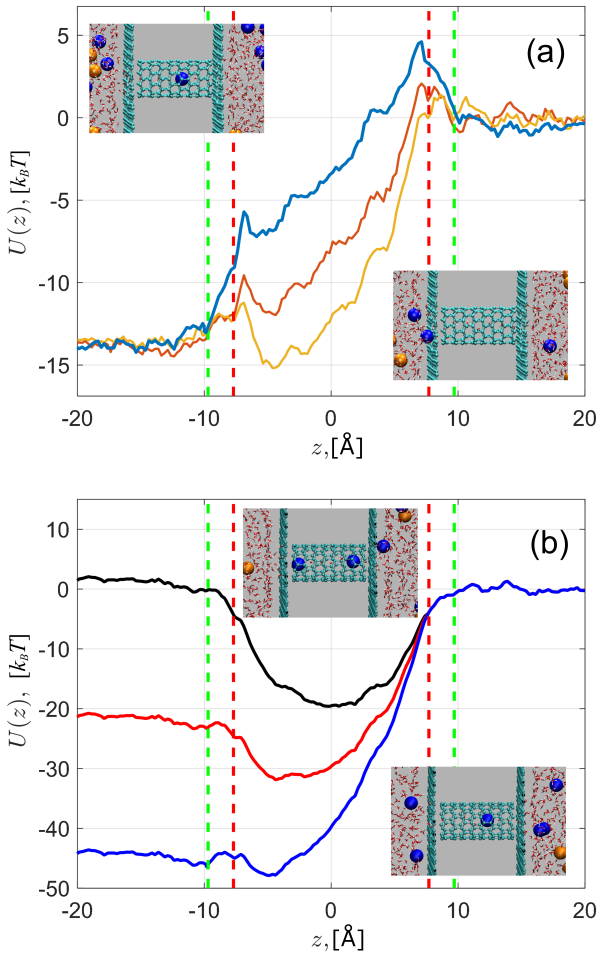

FIG. 4. (a) One-dimensional PMF of a K^+ ion along the z-axis of the CNT. Initially, on the extreme left, the ion is outside the CNT. All other ions are spherically restrained from the tube. The PMFs were calculated for a bias field of 0.04 V/nm, for $Q_{ex} = -1.4e$ (blue curve), $-1.6e$ (brown curve) and $-1.8e$ (yellow curve). Vertical dashed lines show the boundaries of the CNT, and green dashed lines show the locations of the graphene sheets. The insets show the CNT in the two states corresponding to the 1 to 0 transition from one ion (top) to zero ions (bottom). (b) 1D PMF of K^+ ion in the channel, with $Q_{ex} = -2.2e$ and applied fields F of 0 V/nm (black curve), 0.04 V/nm (red), and 0.08 V/nm (blue). The insets show the CNT in the two states corresponding to the $(2 \to 1)'$ transition from two ions (top) to one ion (bottom). The ions are coloured as in Fig. 2.

at nearly constant occupancy of the CNT and is therefore one of the secondary peaks. During this transition the 3-rd ion enters the channel mouth and remotely knocks out the rightmost ion from the CNT. Similarly to the case $(2 \to 1)'$, such intrusions are very brief in time and the CNT predominantly contains only two ions. However, the channel mouth occupancy may increase significantly as shown by the cyan diamonds in Fig. 3 supporting the idea of this remote knock-on mechanism: see also video No. 4 of the SM. The intensity of these peaks is determined by a nontrivial interplay of the applied field, dehydration barrier, and wall charge. They can

be partially or completely suppressed for some model parameters, including changes of the applied field and/or scaling of the ionic charge[58].

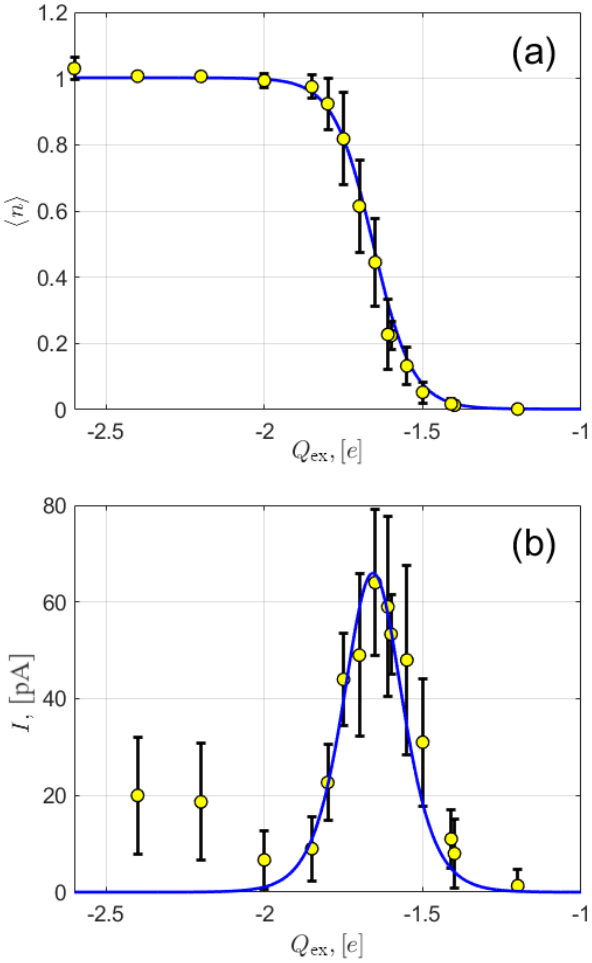

FIG. 5. Comparison of the population (a) and current (b) measured in the MD simulations (yellow circles) with predictions of the ICB theory (solid blue lines).

The ICB theory is an excellent agreement with obtained results as illustrated in Fig. 5. The key parameters of the system can be estimated by fitting MD data including the charging energy U_c, the dehydration energy of the ions in the channel $\Delta\bar{\mu}_b$, the capacitance C, and the diffusivity of the ions in the channel D_c. Indeed, the occupancy and the current at the first peak measured for applied field 0.04 V/nm shown in the Fig. 3 (b) (see the discussion in the SM Secs. I and III) are given by:

$$\begin{aligned} \langle n \rangle &= (1+\exp[\Delta G/k_B T])^2; \\ I &= \frac{q^2 \pi D_c}{8L^2 k_B T} \cosh^{-2}(\Delta G/k_B T)\delta\phi. \end{aligned} \tag{2}$$

By fitting MD data with the equations (2) the values of parameters can be estimated as follows: $U_c \sim 8\ k_B T$, $\Delta\bar{\mu}_* \sim -14\ k_B T$, and $D_c \sim 10^{-10}$ m^{2}s^{-1}, and $C_{dot} \sim 10^{-19}$ F. As discussed in the SM Sec. I the model is quite sensitive to the changes of these parameters. We note that the parameter $\Delta\bar{\mu}^* = \Delta\bar{\mu}^b + \Delta U_{LJ} + \Delta U_{pore}$ represents contributions from three different competing mechanisms involved into the ion conduction including changes in excess chemical potential, Lennard-Jones interactions, and the Coulomb interaction with charges on the pore rims. All three contributions could be resolved by measurements of the system PMFs as discussed in the SM Sec. III and estimated as $\Delta U_{LJ} \sim -10\ k_B T$, $\Delta U_{PMF,pore} \sim -9\ k_B T$, and $\Delta\bar{\mu} \sim -33\ k_B T$. We emphasise that the obtained results reveal values of the key physical parameters of the ICB model of ion conduction through the CNT.

We note the observation of Li *et al.*[59] that a polarizable force field was needed for ions to enter the channel. In the present work we have found, however, that the charge on the CNT reduces the dehydration barrier sufficiently for the charge to enter, without use of polarizable force field. The origin of this apparent discrepancy is currently unclear, but it is evident that there is some interesting physics here that we intend to explore in the near future.

IV. CONCLUSIONS

In conclusion, our all-atom MD simulations of the ionic current through a short, single-walled, CNT with charged walls have revealed ICB oscillations and an occupancy staircase. Although both effects had been predicted by ICB theory,[15,16,18,27,52] neither had previously been demonstrated in a CNT.

We have shown, however, that the current peaks as a function of the Q_{ex} are attributable to two distinct conduction mechanisms. The first, corresponding to the set of transitions denoted $\{n+1\} \to \{n\}$ occur at occupancy steps, as predicted by the ICB theory. During this type of transition, the CNT is occupied by either by n or by $(n+1)$ ions, with equal probability, i.e. $P_n \approx P_{n+1}$. The second mechanism corresponds to the transitions denoted $(\{n+1\} \to \{n\})'$ that occur at constant occupancy of the CNT. This latter type of transition contradicts expectations based on ICB theory. We showed that the CNT is then predominantly occupied by n ions ($P_{n+1} \ll P_n$), and knock-on is accomplished remotely by a ion arriving transiently at the channel mouth. This type of transition varies in probability and can be attenuated or eliminated for certain choices of model parameters.

These discoveries confirm the conjecture that the ICB plays a fundamental role in controlling ionic conduction in artificial, as well as biological, nanochannels. The new insights pave the way to systematic studies of a wide range of important physical phenomena through their individual effects on ICB oscillations. These include dehydration, wall fluctuations, local dielectric permittivity, wall functionalisation, polarisation, channel mouth geometry, and other physical properties. Systems of the type described by Pang *et al.*[39] and Rabinowitz *et al.*[40] appear to be suitable for experimental tests. We comment also that the system considered here is an excellent candidate for mimicking the celebrated selectivity and conductivity properties of KcsA-like biological channels[60–63].

We aim to extend our studies of ICB oscillations to encompass longer CNTs, a the role of the charged vestibules at the CNT entrances, and DNA sequencing in short CNTs.

The results reported promise to facilitate the design and optimisation of the controllable nanoscale ionic devices needed for e.g. blue energy harvesting[64], DNA sequencing[36], nanofluidic neuromorphic computing[65], ionotronics[66], medical dialysis[67], biosensing[68], and biointerfacing[69].

SUPPLEMENTARY ONLINE MATERIAL

The Supplementary Material PDF document provided with this paper includes: (i) a summary of the statistical theory of ionic Coulomb blockade; (ii) a description of the charge distribution on the CNT and on the adjacent graphene sheets; (iii) a discussion of the use of the potential of the mean force in molecular dynamics computations; and (iv) a detailed discussion of the remote knock-on permeation process.

In addition to the PDF, there are the 4 videos alluded to in the main paper showing how one or more K^+ ions permeate the CNT. Each of them is for rim atom charge $Q_{\rm np} = -1.92e$:

1. Permeation dynamics for a single-ion transition $(1 \to 0)$; $Q_{\rm ex} = -1.60e$ and voltage $F = 0.04$ V/nm.
2. Permeation dynamics for knock-on transition $(2 \to 1)'$; $Q_{\rm ex} = -2.20e$ and voltage $F = 0.08$ V/nm.
3. Permeation dynamics for knock-on transition $(2 \to 1)$; $Q_{\rm ex} = -3.60e$ and voltage $F = 0.08$ V/nm.
4. Permeation dynamics for knock-on transition $(3 \to 2)'$; $Q_{\rm ex} = -4.40e$ and voltage $F = 0.04$ V/nm.

ACKNOWLEDGEMENTS

We are grateful to the J-OCTA team for providing J-OCTA software, for support, and for valuable discussions. This work was supported: by the Leverhulme Trust (UK) [grant number RPG-2017-134]; and by the Engineering and Physical Sciences Research Council (UK) [grant number EP/M015831/1].

AUTHOR DECLARATIONS

Conflict of interest

The authors have no conflicts to declare.

Author contributions

William A. T. Gibby: Conceptualization (equal); Formal analysis (equal); Investigation (equal); Writing – original draft (equsl); Writing – review & editing (equal). **Miraslau L. Barabash**: Conceptualization (equal); Formal analysis (equal); Investigation (equal); Writing – original draft (equsl); Writing – review & editing (equal). **Igir A. Khovanov**: Conceptualization (equal); Formal analysis (equal); Funding acquisition (equal); Investigation (equal); Writing – original draft (equsl); Writing – review & editing (equal). **Dmitri G. Luchinsky**: Conceptualization (lead); Formal analysis (equal); Funding acquisition (equal); Investigation (lead); Writing – original draft (equsl); Writing – review & editing (equal). **Peter V. E. McClintock**: Funding acquisition (equal); Investigation (equal); Project administration (equal); Supervision (equal); Writing – review & editing (equal).

REFERENCES

[1] B. Hille, *Ion Channels Of Excitable Membranes*, 3rd ed. (Sinauer Associates, Sunderland, MA, 2001).
[2] F. M. Ashcroft, *Ion Channels and Disease* (Academic Press, London, 1999).
[3] X. Huang and L. Y. Jan, "Targeting potassium channels in cancer," J. Cell Biol. **206**, 151–162 (2014).
[4] J. Comer and A. Aksimentiev, "DNA sequence-dependent ionic currents in ultra-small solid-state nanopores," Nanoscale **8**, 9600–9613 (2016).
[5] J. Feng, M. Graf, K. Liu, D. Ovchinnikov, D. Dumcenco, M. Heiranian, V. Nandigana, N. R. Aluru, A. Kis, and A. Radenovic, "Single-layer MoS2 nanopores as nanopower generators," Nature **536**, 197–200 (2016).
[6] M. Macha, S. Marion, V. V. R. Nandigana, and A. Radenovic, "2D materials as an emerging platform for nanopore-based power generation," Nat. Rev. Mater. **4**, 588–605 (2019).
[7] A. Fang, K. Kroenlein, D. Riccardi, and A. Smolyanitsky, "Highly mechanosensitive ion channels from graphene-embedded crown ethers," Nat. Mater. **18**, 76–81 (2019).
[8] H. Du, J. Li, J. Zhang, G. Su, X. Li, and Y. Zhao, "Separation of hydrogen and nitrogen gases with porous graphene membrane," J. Phys. Chem. C **115**, 23261–23266 (2011), https://doi.org/10.1021/jp206258u.
[9] M. Lozada-Hidalgo, S. Hu, O. Marshall, A. Mishchenko, A. N. Grigorenko, R. A. W. Dryfe, B. Radha, I. V. Grigorieva, and A. K. Geim, "Sieving hydrogen isotopes through two-dimensional crystals," Science **351**, 68–70 (2016), https://science.sciencemag.org/content/351/6268/68.full.pdf.
[10] L. Wang, M. S. Boutilier, P. R. Kidambi, D. Jang, N. G. Hadjiconstantinou, and R. Karnik, "Fundamental transport mechanisms, fabrication and potential applications of nanoporous atomically thin membranes," Nat. Nanotechnol. **12**, 509 (2017).
[11] B. Roux, "Ion channels and ion selectivity," Essays Biochem. **61**, 201–209 (2017).
[12] S. Faucher, N. Aluru, M. Z. Bazant, D. Blankschtein, A. H. Brozena, J. Cumings, J. Pedro de Souza, M. Elimelech, R. Epsztein, J. T. Fourkas, A. G. Rajan, H. J. Kulik, A. Levy, A. Majumdar, C. Martin, M. McEldrew, R. P. Misra, A. Noy, T. A. Pham, M. Reed, E. Schwegler, Z. Siwy, Y. Wang, and M. Strano, "Critical knowledge gaps in mass transport through single-digit nanopores: A review and perspective," J. Phys. Chem. C **123**, 21309–21326 (2019).
[13] N. R. Aluru, F. Aydin, M. Z. Bazant, D. Blankschtein, A. H. Brozena, J. P. de Souza, M. Elimelech, S. Faucher, J. T. Fourkas, V. B. Koman, M. Kuehne, H. J. Kulik, H.-K. Li, Y. Li, Z. Li, A. Majumdar, J. Martis, R. P. Misra, A. Noy, T. A. Pham, H. Qu, A. Rayabharam, M. A. Reed, C. L. Ritt, E. Schwegler, Z. Siwy, M. S. Strano, Y. Wang, Y.-C. Yao, C. Zhan, and Z. Zhang, "Fluids and electrolytes under confinement in single-digit nanopores," Chem. Rev. **123**, 2737–2831 (2023), pMID: 36898130, https://doi.org/10.1021/acs.chemrev.2c00155.
[14] M. Krems and M. D. Ventra, "Ionic Coulomb blockade in nanopores," J. Phys: Cond. Matt. **25**, 065101 (2013).
[15] I. K. Kaufman, D. G. Luchinsky, R. Tindjong, P. V. E. McClintock, and R. S. Eisenberg, "Multi-ion conduction bands in a simple model of calcium ion channels," Phys. Biol. **10**, 026007 (2013).
[16] I. K. Kaufman, P. V. E. McClintock, and R. S. Eisenberg, "Coulomb blockade model of permeation and selectivity in biological ion channels," New J. Phys. **17**, 083021 (2015).

[17] J. Feng, K. Liu, M. Graf, D. Dumcenco, A. Kis, M. Di Ventra, and A. Radenovic, "Observation of ionic coulomb blockade in nanopores," Nat. Mater. **15**, 850–855 (2016).
[18] N. Kavokine, S. Marbach, A. Siria, and L. Bocquet, "Ionic Coulomb blockade as a fractional Wien effect," Nat. Nanotechnol. **14**, 573–578 (2019).
[19] C. Beenakker, "Theory of Coulomb-blockade oscillations in the conductance of a quantum dot," Phys. Rev. B **44**, 1646–1656 (1991).
[20] J. G. Lu, "Single electronics," in *Introduction to Nanoscale Science and Technology*, edited by M. Di Ventra, S. Evoy, and J. R. Heflin (Springer US, Boston, MA, 2004) pp. 261–312.
[21] B. I. Halperin, "Electronic properties of nanoparticles and nanostructures," `https://projects.iq.harvard.edu/files/nsec/files/17-halperin.ap298rtalk.pdf` (2005), accessed: 2010-09-30.
[22] K. Miyaji and T. Hiramoto, "Silicon single electron transistors operating at room temperature and their applications," in *Comprehensive Semiconductor Science and Technology* (Elsevier, 2011) p. 340–382.
[23] Y. V. Nazarov, "Coulomb blockade," in *Encyclopedia of Condensed Matter Physics* (Second Edition), Vol. 3 (Elsevier, 2024) pp. 260–272.
[24] Wikipedia, "Coulomb blockade," (2021), page Version ID: 1046852115.
[25] H. Van Houten, C. W. J. Beenakker, and A. A. M. Staring, "Coulomb-blockade oscillations in semiconductor nanostructures," in *Single Charge Tunneling: Coulomb Blockade Phenomena In Nanostructures*, edited by H. Grabert and M. H. Devoret (Springer US, Boston, MA, 1992) pp. 167–216.
[26] L. P. Kouwenhoven, C. M. Marcus, P. L. McEuen, S. Tarucha, R. M. Westervelt, and N. S. Wingreen, "Electron transport in quantum dots," in *Mesoscopic Electron Transport*, edited by L. L. Sohn, L. P. Kouwenhoven, and G. Schön (Springer Netherlands, Dordrecht, 1997) pp. 105–214.
[27] W. A. T. Gibby, M. L. Barabash, C. Guardiani, D. G. Luchinsky, and P. V. E. McClintock, "Physics of selective conduction and point mutation in biological ion channels," Phys. Rev. Lett. **126**, 218102 (2021).
[28] A. Radenovic, "Prospects of observing ionic Coulomb blockade in artificial ion confinements," Entropy **22**, 1430 (2020).
[29] O. A. Fedorenko, I. K. Kaufman, W. A. T. Gibby, M. L. Barabash, D. G. Luchinsky, S. K. Roberts, and P. V. E. McClintock, "Ionic Coulomb blockade and the determinants of selectivity in the NaChBac bacterial sodium channel," BBA – Biomembranes **1862**, 183301 (2020).
[30] A. Smolyanitsky, A. Fang, A. F. Kazakov, and E. Paulechka, "Ion transport across solid-state ion channels perturbed by directed strain," Nanoscale **12**, 10328–10334 (2020).
[31] A. Smolyanitsky, E. Paulechka, and K. Kroenlein, "Aqueous ion trapping and transport in graphene-embedded 18-crown-6 ether pores," ACS Nano **12**, 6677–6684 (2018).
[32] S. Sahu, J. Elenewski, C. Rohmann, and M. Zwolak, "Optimal transport and colossal ionic mechano-conductance in graphene crown ethers," Sci. Adv. **5**, eaaw5478 (2019).
[33] C. Guardiani, W. A. T. Gibby, M. L. Barabash, D. G. Luchinsky, and P. V. E. McClintock, "Exploring the pore charge dependence of K^+ and Cl^- permeation across a graphene monolayer: a molecular dynamics study," RSC Adv. **9**, 20402–20414 (2019).
[34] Z. He, J. Zhou, X. Lu, and B. Corry, "Bioinspired graphene nanopores with voltage-tunable ion selectivity for Na^+ and K^+," ACS Nano **7**, 10148–10157 (2013).
[35] X. Gong, J. Li, K. Xu, J. Wang, and H. Yang, "A controllable molecular sieve for Na^+ and K^+ ions," J. Am. Chem. Soc. **132**, 1873–1877 (2010).
[36] L. Liu, C. Yang, K. Zhao, J. Li, and H.-C. Wu, "Ultrashort single-walled carbon nanotubes in a lipid bilayer as a new nanopore sensor," Nat. Comm. **4**, 10.1038/ncomms3989 (2013).
[37] M. P. Aranha and B. J. Edwards, "Ion transport through single-walled carbon nanotubes: Effects of electric field and fixed surface charge," Chem. Phys. Lett. **712**, 95–101 (2018).
[38] S. Zhang, L. Fu, and Y. Xie, "Ionic blockade in a charged single-file water channel," arXiv preprint arXiv:2304.13355 [cond-mat.soft] (2023).
[39] P. Pang, J. He, J. H. Park, P. S. Krstić, and S. Lindsay, "Origin of giant ionic currents in carbon nanotube channels," ACS Nano **5**, 7277–7283 (2011).
[40] J. Rabinowitz, C. Cohen, and K. L. Shepard, "An electrically actuated, carbon-nanotube-based biomimetic ion pump," Nano Lett. **20**, 1148–1153 (2019).
[41] A. B. Farimani, M. Heiranian, and N. R. Aluru, "Nano-electro-mechanical pump: Giant pumping of water in carbon nanotubes," Sci. Rep. **6**, 26211 (2016).
[42] W. Zhou, Y. Y. Wang, T.-S. Lim, T. Pham, D. Jain, and P. J. Burke, "Detection of single ion channel activity with carbon nanotubes," Sci. Rep. **5**, 9208 (2015).
[43] W. L. Jorgensen, J. Chandrasekhar, J. D. Madura, R. W. Impey, and M. L. Klein, "Comparison of simple potential functions for simulating liquid water," J. Chem. Phys. **79**, 926–935 (1983).
[44] I. S. Joung and T. E. Cheatham, "Determination of alkali and halide monovalent ion parameters for use in explicitly solvated biomolecular simulations," J. Phys. Chem. B **112**, 9020–9041 (2008).
[45] *User's Manual, J-OCTA Overview, J-OCTA 4.0*, JSOL Corp. (2018).
[46] Case, D. A. *et. al.*, *Amber 2023 Reference Manual* (University of California, San Francisco, 2023).
[47] S. L. Mayo, B. D. Olafson, and W. A. Goddard, "DREIDING: a generic force field for molecular simulations," J. Phys. Chem. **94**, 8897–8909 (1990), http://dx.doi.org/10.1021/j100389a010.
[48] E. Lindahl, B. Hess, and D. van der Spoel, "GROMACS 3.0: a package for molecular simulation and trajectory analysis," J. Mol. Model. **7**, 306–317 (2001).
[49] A. Barducci, G. Bussi, and M. Parrinello, "Well-tempered metadynamics: A smoothly converging and tunable free-energy method," Phys. Rev. Lett. **100**, 020603 (2008).
[50] G. Fiorin, M. L. Klein, and J. Hénin, "Using collective variables to drive molecular dynamics simulations," Mol. Phys. **111**, 3345–3362 (2013).
[51] W. Humphrey, A. Dalke, and K. Schulten, "VMD: Visual molecular dynamics," J. Mol. Graph. **14**, 33 – 38 (1996).
[52] O. A. Fedorenko, I. K. Kaufman, W. A. T. Gibby, D. G. Luchinsky, S. K. Roberts, and P. V. E. McClintock, "Quantized dehydration and the determinants of selectivity in the NaChBac bacterial sodium channel," arXiv preprint arXiv:1803.07063 (2018).
[53] D. G. Luchinsky, W. A. T. Gibby, I. Kaufman, D. A. Timucin, and P. V. E. McClintock, "Statistical theory of selectivity and conductivity in biological channels," arXiv preprint arXiv:1604.05758 (2016).
[54] R. Tindjong, I. Kh. Kaufman, D. G. Luchinsky, P. V. E. McClintock, I. A. Khovanov, and R. S. Eisenberg, "Stochastic dynamics of remote knock-on permeation in biological ion channels," in *22nd Intern. Conf. on Noise and Fluctuations (ICNF),* Montpellier, 24–28 June 2013 (IEEE Conference Proceedings, 2013) p. 10.1109/ICNF.2013.6578893.
[55] R. Tindjong, I. K. Kaufman, D. G. Luchinsky, P. V. E. McClintock, I. Khovanov, and R. S. Eisenberg, "Self-organized enhancement of conductivity in biological ion channels," New J. Phys. **15**, 103005 (2013).
[56] D. G. Luchinsky, R. Tindjong, I. Kaufman, P. V. E. McClintock, and R. S. Eisenberg, "Ion channels as electrostatic amplifiers of charge fluctuations," J. Phys.: Conference Series **142**, 012049 (2008).
[57] F. T. Heer, D. J. Posson, W. Wojtas-Niziurski, C. M. Nimigean, and S. Bernèche, "Mechanism of activation at the selectivity filter of the KcsA k^+ channel," eLife **6**, 10.7554/elife.25844 (2017).
[58] G. D. Barbosa, X. Liu, K. E. O'Harra, J. E. Bara, and C. H. Turner, "Charge scaling parameter evaluation for multivalent ionic liquids with fixed point charge force fields," J. Ionic Liq. **2**, 100020 (2022).
[59] Z. Li, R. P. Misra, Y. Li, Y.-C. Yao, S. Zhao, Y. Zhang, Y. Chen, D. Blankschtein, and A. Noy, "Breakdown of the Nernst–Einstein relation in carbon nanotube porins," Nat. Nanotech. **18**, 177–183 (2023).
[60] D. A. Doyle, J. M. Cabral, R. A. Pfuetzner, A. Kuo, J. M. Gulbis, S. L. Cohen, B. T. Chait, and R. MacKinnon, "The structure of the potassium channel: Molecular basis of K^+ conduction and selectivity," Science **280**, 69–77 (1998).
[61] J. H. H. Morais-Cabral, Y. Zhou, and R. MacKinnon, "Energetic optimization of ion conduction rate by the K^+ selectivity filter," Nature **414**, 37–42 (2001).
[62] D. A. Köpfer, C. Song, T. Gruene, G. M. Sheldrick, U. Zachariae, and B. L. de Groot, "Ion permeation in K^+ channels occurs by direct Coulomb knock-on," Science **346**, 352–355 (2014).
[63] W. Kopec, D. A. Köpfer, O. N. Vickery, A. S. Bondarenko, T. L. Jansen, B. L. de Groot, and U. Zachariae, "Direct knock-on of desolvated ions governs strict ion selectivity in K^+ channels," Nat. Chem. **10**, 813–820 (2018).
[64] M. Graf, M. Lihter, D. Unuchek, A. Sarathy, J.-P. Leburton, A. Kis, and A. Radenovic, "Light-enhanced blue energy generation using MoS_2 nanopores," Joule **3**, 1549–1564 (2019).

[65]T. M. Kamsma, J. Kim, K. Kim, W. Q. Boon, C. Spitoni, J. Park, and R. van Roij, "Brain-inspired computing with fluidic iontronic nanochannels," arXiv preprint arXiv:2309.11438 [cond-mat.soft] (2023).

[66]R. Peng, Y. Pan, Z. Li, S. Zhang, A. R. Wheeler, X. S. Tang, and X. Liu, "Ionotronics based on horizontally aligned carbon nanotubes," Adv. Funct. Mat. **30**, 2003177 (2020), https://onlinelibrary.wiley.com/doi/pdf/10.1002/adfm.202003177.

[67]Y. Xue, Y. Xia, S. Yang, Y. Alsaid, K. Y. Fong, Y. Wang, and X. Zhang, "Atomic-scale ion transistor with ultrahigh diffusivity," Science **372**, 501–503 (2021), https://www.science.org/doi/pdf/10.1126/science.abb5144.

[68]L. Steller, M. Kreir, and R. Salzer, "Natural and artificial ion channels for biosensing platforms," Anal.Bioanalytic. Chem. **402**, 209–230 (2011).

[69]T. Sarkar, K. Lieberth, A. Pavlou, T. Frank, V. Mailaender, I. McCulloch, P. W. M. Blom, F. Torricelli, and P. Gkoupidenis, "An organic artificial spiking neuron for *in situ* neuromorphic sensing and biointerfacing," Nat. Electron. **5**, 774–783 (2022).